Role of Reflective (Metallic) Support on Microwave Heating

Tanmay Basak
Dept. of Chemical Engineering, Indian Institute of Technology, Madras, Chennai 600 036, India

DOI 10.1002/aic.10463
Published online March 30, 2005 in Wiley InterScience (www.interscience.wiley.com).

A detailed analysis has been carried out to assess the role of reflective support on microwave heating of one-dimensional (1-D) slabs and 2-D cylinders for water and oil samples. The reflective supports are placed at the unexposed face for 1-D slabs, and the supports are the annular cylinders with specific radii for 2-D cylinders. A preliminary analysis on microwave heating of samples has been shown via average power within a sample vs sample dimension diagram for various regimes. For 1-D water samples, the regime I corresponds to local maxima in average power for samples with supports, and regime II corresponds to maxima in power for samples without supports. For 1-D oil samples, the greater average power with supports during regimes I and II is observed. The enhanced power absorption is observed due to greater stationary field intensities, and the greater heating rates are due to the enhanced power deposition in samples with supports for specific regimes. For 2-D water samples, the reflective supports are found to be attractive for specific aspects ratios and power absorption can be enhanced by several magnitudes for thicker cylinder radii. The power absorption is found to be generally decreased due to supports for 2-D oil samples. © 2005 American Institute of Chemical Engineers *AIChE J,* 51: 1319–1329, 2005
Keywords: microwave, reflective support, slabs, cylinders

Introduction

Due to volumetrically heating effects, microwaves (MWs) are largely applied in various industries such as heating and thawing of materials; food processing; drying; sintering of ceramics; polymer processing and many more (Weil, 1975; Ayappa et al., 1992; Chatterjee et al., 1998; Chamchong and Datta, 1999; Basak and Ayappa, 1997, 2001; Zhang et al., 2001; Sivalingam et al., 2003; Lee and Marchant, 2004). MWs penetrate within the material and depending on the sample size, the incident uniform plane wave may be decomposed into reflected and transmission waves at various material boundaries (Ayappa et al., 1991; Basak, 2003; Basak, 2004). For a small sample size, the oscillatory behavior of microwaves is observed due to the standing waves, based on interference of reflected and transmitted waves. In contrast, for a large sample size, the microwaves decay exponentially within the medium where the reflection is totally absent.

During customized plane wave heating, the constructive interferences of traveling waves result in greater heating effects corresponding to specific sample lengths (Barringer et al., 1994). The constructive interference of the traveling waves is often termed as "Resonances" which may be illustrated by the local maxima in average power absorption vs sample dimension plot, and the spatial distribution of absorbed power is deduced by solving Maxwell's equations. The associated temperature rise in the sample is obtained by an appropriate energy balance. The resonance in average power corresponds to greater spatial power deposition, and the spatial resonance in a sample can be quantified as the zero phase difference between the traveling waves. The minima in average power occurs between two consecutive resonances and the minima results in lower heating effects. In short, the oscillatory features in power absorption may provide strategic guideline in processing the samples for specific sample sizes. The oscillatory power ab-

T. Basak's e-mail address is tanmay@iitm.ac.in.

sorption for thin slabs are extensively investigated via a number of patents (Peschek et al., 1992). Considerable earlier investigations were carried out to analyze the oscillatory heating characteristics and resonances for various geometries.

A number of studies was carried out to analyze microwave heating by earlier researchers to investigate heating patterns in 1-D slabs and 2-D cylinders (Ohlsson and Risman, 1978; Jolly and Turner, 1990; Ayappa et al., 1991, 1992; Barringer et al., 1994; Basak and Ayappa, 1997, 2001, 2002). Ohlsson and Risman (1978) observed resonances while carrying out MW heating experiments in cylindrical and spherical samples at 2450 MHz. Jolly and Turner (1990) carried out theoretical studies to investigate resonance for 1-D slabs, and they observed a runaway situation during resonance. Ayappa et al. (1991, 1992) carried out theoretical and numerical studies on MW heating of 1-D slabs and 2-D cylinders, and they observed a greater heating rate for thinner samples while heating occurs primarily at the incident face for thicker samples. Basak and Ayappa (1997, 2001, 2002) carried out MW thawing for 1-D slabs and 2-D cylinders of pure and multicomponent samples, and they observed a greater melting rate during resonances. They also observed multiple melting fronts for thinner cylinders corresponding to greater thawing rates. The counterintuitive situation, such as thicker samples taking less time to thaw than thinner samples in the presence of resonance, was recently analyzed by Basak (2003). A detailed analysis on resonances for heating of emulsions are also recently addressed by Basak (2004).

The extensive studies on MW heating are mainly devoted to analyze enhanced thermal effects during resonances which are strong functions of sample size. Microwaves are wastefully used in absence of resonances, where the traveling waves are destructive to each other. The application of foreign reflective (metallic) support may be useful to focus MWs for a controlled heating which was earlier carried out by a very few researchers. Jolly and Turner (1990) carried out preliminary studies on MW heating with reflective supports, where they used the reflective support to control the temperature as the MW power is zero within the metallic (reflective) support. Ayappa (1999) carried out the resonance studies of 1-D slabs with a metallic support at the unexposed face. The potential use of metallic support on enhanced or controlled MW heating is poorly understood till date. A detailed analysis on enhanced heating with some reflective support would be a significant addition in the literature to address the potential enhancement of MW usage, efficient strategies and controlled heating procedures.

Here we carry out a detailed analysis on oscillatory behavior of MW incidences and the enhanced use of MW heating for samples with reflective supports. A mathematical analysis on spatial power distributions has been carried out for 1-D slabs with/without reflective supports. MW propagation within a sample is governed by Maxwell's equations whose solution is a linear combination of the traveling waves due to transmission and reflection. An analytical solution has been developed to study the influence of traveling waves on MW power distributions for a system. The average power is evaluated for various sample thicknesses either for cases without support or with support and it is observed that a minima in average power for 1-D slabs without support corresponds to a maxima in average power with reflective support for specific cases. A detailed analysis on resonances for various regimes with/without supports are also carried out to illustrate the efficient use of MWs for various sample thicknesses.

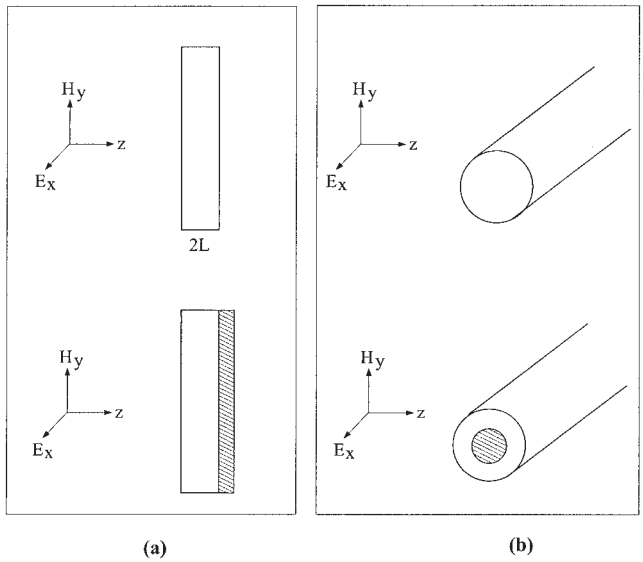

Figure 1. (a) 1-D slab, and (b) 2-D cylinder exposed to plane electromagnetic waves.

The shaded region denotes the reflective support.

Microwave heating is modeled with an energy balance equation, where heat generation due MW power is a function of electric fields. The heating of samples without support is contrasted with the samples on reflective support and for all cases, based on greater material processing rates, the processing lengths are recommended. The studies on 1-D slabs are extended for 2-D cylinders with annular reflective support. The enhanced MW power absorption is illustrated for various aspect ratios.

Theory

Evaluation of Electric fields and Microwave Power: Analysis in a multilayered 1-D slab

The wave propagation due to uniform electric field E_x within a medium is governed by (Ayappa et al., 1991)

$$\frac{d^2E_x}{dz^2} + k^2E_x = 0 \tag{1}$$

where E_x lies in $x - y$ plane and varies only along the direction of propagation, z axis (Figure 1a) and the propagation constant

$$k = \frac{\omega}{c}\sqrt{\kappa' + i\kappa''} \tag{2}$$

depends on the dielectric constant, κ' and the dielectric loss, κ''. Here $\omega = 2\pi f$, where f is the frequency of the electromagnetic wave, and c is the velocity of light. As seen in Figure 1a the 1-D slab is either surrounded by the air medium (when the slab has no support), or the slab may have a reflective support at the unexposed surface and the electric field distribution for the l_{th} medium in a composite obtained from Eq. 1 is

$$\frac{d^2E_{x,l}}{dz^2} + k_l^2 E_{x,l} = 0 \tag{3}$$

where $z_{l-1} \le z \le z_l$ and $l = 1 - 3$. Note that, $l = 1, 3$ denote air medium, $l = 2$ denotes the sample and the reflective support may be denoted as $l = 3$. We assume each layer has constant dielectric properties and hence, the general solution to Eq. 3 represented as a linear combination of traveling waves propagating in opposite directions is

$$E_{x,1} = E_{t,1}e^{ik_1 z} + E_{r,1}e^{-ik_1 z} \quad z \le z_1$$

$$E_{x,2} = E_{t,2}e^{ik_2 z} + E_{r,2}e^{-ik_2 z} \quad z_1 \le z \le z_2$$

$$E_{x,3} = \begin{cases} E_{t,3}e^{ik_3 z} + E_{r,3}e^{-ik_3 z}, & z \ge z_2 \text{ (air)} \\ 0, & z \ge z_2 \text{ (reflective support)} \end{cases} \tag{4}$$

where $E_{t,l}$ and $E_{r,l}$ are the coefficients due to transmission and reflection, respectively. The boundary conditions at the interface are

$$\left.\begin{aligned} E_{x,l-1} &= E_{x,l} \\ \frac{dE_{x,l-1}}{dz} &= \frac{dE_{x,l}}{dz} \end{aligned}\right\} \begin{aligned} l &= 2, 3 \\ z &= z_1, z_2 \end{aligned} \tag{5}$$

Using the interface conditions (Eq. 5) and the general solutions (Eq. 4), the coefficients, $E_{t,l}$ and $E_{r,l}$ are obtained via solving the set of algebraic equations

$$\left.\begin{aligned} E_{t,l}e^{ik_l z_l} + E_{r,l}e^{-ik_l z_l} - E_{t,l+1}e^{ik_{l+1} z_l} - E_{r,l+1}e^{-ik_{l+1} z_l} &= 0 \\ k_l E_{t,l}e^{ik_l z_l} - k_l E_{r,l}e^{-ik_l z_l} - k_{l+1}E_{t,l+1}e^{ik_{l+1} z_l} + k_{l+1}E_{r,l+1}e^{-ik_{l+1} z_l} &= 0 \end{aligned}\right\} l = 1, 2 \tag{6}$$

As the incident field intensities from the source is known, that is, $E_{t,1} = E_0$, for the third medium, $E_{r,3} = 0$, and for reflective support, $E_{x,3} = 0$, therefore, Eqs. 6 are solved for the remaining coefficients, following the similar manner as discussed by Basak (2003). For the l_{th} layer, the transmitted and reflected waves are

$$E_{x,l}^t = E_{t,l}e^{ik_l z} = A_{x,l}^t e^{i\delta_{x,l}^t}$$

$$E_{x,l}^r = E_{r,l}e^{-ik_l z} = A_{x,l}^r e^{i\delta_{x,l}^r} \tag{7}$$

where corresponding amplitudes

$$A_{x,l}^t = \sqrt{E_{x,l}^t E_{x,l}^t{}^*}$$

$$A_{x,l}^r = \sqrt{E_{x,l}^r E_{x,l}^r{}^*} \tag{8}$$

and the phase states

$$\delta_{x,l}^t = \tan^{-1}\left[\frac{\mathrm{Im}(E_{x,l}^t)}{\mathrm{Re}(E_{x,l}^t)}\right]$$

$$\delta_{x,l}^r = \tan^{-1}\left[\frac{\mathrm{Im}(E_{x,l}^r)}{\mathrm{Re}(E_{x,l}^r)}\right] \tag{9}$$

where the superscript '*' in Eq. 8 denotes the complex conjugate. For a stationary wave in the l^{th} layer, the amplitude is

$$A_{x,l} = \sqrt{E_{x,l}E_{x,l}^*} \tag{10}$$

and the difference in phase angle

$$\delta_{x,l} = \delta_{x,l}^t - \delta_{x,l}^r \tag{11}$$

where the quantities $E_{x,l}$ and $E_{x,l}^*$ appeared in Eq. 10 are evaluated using Eqs. 4 and 7. At the resonance, the difference in phase angle is zero, that is, $\delta_{x,l} = 0$. For a given flux of incident radiation, I_0, in free space the incident electric field intensity E_0, is given by

$$E_0 = \sqrt{\frac{2I_0}{c\varepsilon_0}}. \tag{12}$$

The power for l_{th} layer, obtained from Poynting vector theorem is

$$q = \frac{1}{2}\,\omega\varepsilon_0\kappa'' E_{x,l}E_{x,l}^*, \tag{13}$$

where ε_0 is the free space permittivity. The dielectric loss κ'' may be assumed as a constant within a sample. The average power obtained by integrating the power across the slab is

$$q_{av} = \frac{1}{2L}\int_{-L}^{L} q(z)dz \tag{14}$$

Here, $2L$ denotes the sample thickness as shown in Figure 1a.

The penetration depth D_p and wavelength of radiation in the medium λ_m are related to κ' and κ'' in the following manner

$$D_p = \frac{c}{\sqrt{2}\,\pi f\left[\kappa'\left(\sqrt{1 + \left(\frac{\kappa''}{\kappa'}\right)^2} - 1\right)\right]^{1/2}} \tag{15}$$

and

$$\lambda_m = \frac{c\sqrt{2}}{f\left[\kappa'\left(\sqrt{1 + \left(\frac{\kappa''}{\kappa'}\right)^2} + 1\right)\right]^{1/2}} \tag{16}$$

The propagation constant in Eq. 1 is

$$k = (2\pi/\lambda_m) + i(1/D_p) \tag{17}$$

Modeling of microwave heating in slabs and cylinders

In this section, we have analyzed heating of 1-D slabs and 2-D cylinders in presence of volumetric heat sources due to microwave propagation within the samples. Microwaves are assumed to be incident normally on the face of the slab as shown in Figure 1a, and on an infinite cylinder as shown in Figure 1b. The incident microwave is a uniform plane wave, with the electric and magnetic components varying in intensity only in the direction of wave propagation (z axis). The heat transport within a sample is governed by an energy balance equation

$$\rho C_p \frac{\partial T}{\partial t} = k\nabla^2 T + q \tag{18}$$

where ρC_p is the specific heat per unit volume, k is the thermal conductivity and q is the absorbed microwave power as given in Eq. 13. The wave propagation due to electric field, E_x, is governed by (Ayappa et al., 1992)

$$\nabla^2 E_x + k^2 E_x = 0 \tag{19}$$

where E_x varies in the $y - z$ plane only as seen in Figure 1 and k is the propagation constant as discussed in Eq. 2.

Using the dimensionless variables

$$u_x = \frac{E_x}{E_0} \text{ and } \nabla^* = D_s\nabla$$

Equation 19 reduces to

$$\nabla^{*2} u_x + \gamma^2 u_x = 0 \tag{20}$$

where u_x is the electric field intensity, $\gamma = (D_s\omega/c)\sqrt{\kappa' + i\kappa''}$ is the propagation constant and $D_s = 2L$ for slabs, $D_s = R$ for 2-D cylinders. Substituting the complex field variable $u_x = v_x + iw_x$ into Eq. 20 and equating the real and imaginary components, we get

$$\nabla^{*2} v_x + \chi_1 v_x - \chi_2 w_x = 0 \tag{21}$$

and

$$\nabla^{*2} w_x + \chi_2 v_x + \chi_1 w_x = 0 \tag{22}$$

with $\chi_1 = (D_s^2\omega^2/c^2)\kappa'$ and $\chi_2 = (D_s^2\omega^2/c^2)\kappa''$.

For uniform plane waves incident on a sample some of the radiation is scattered and the rest is absorbed. For 1-D slab, boundary conditions (Basak and Ayappa, 1997) for the real and imaginary components during MW incidence of samples without any supports are

$$\left.\begin{aligned} \frac{dv_x}{dz'} - \frac{2\omega L}{c}\omega_x &= \frac{4\omega L}{c}\sin\left(\frac{\omega L}{c}\right) \\ \frac{dw_x}{dz'} + \frac{2\omega L}{c}v_x &= \frac{4\omega L}{c}\cos\left(\frac{\omega L}{c}\right) \end{aligned}\right\} \text{at } z' = 0 \tag{23}$$

and

$$\left.\begin{aligned} \frac{dv_x}{dz'} + \frac{2\omega L}{c}w_x &= 0 \\ \frac{dw_x}{dz'} - \frac{2\omega L}{c}v_x &= 0 \end{aligned}\right\} \text{at } z' = 1 \tag{24}$$

Here, the dimensionless variable, $z' = (z + L)/2L$).

Radiation boundary conditions (Ayappa et al., 1992) used at the outer surface of the cylinder are

$$\begin{aligned} \mathbf{n}\cdot\nabla^* v_x = &\sum_{n=0}^{\infty} \mathrm{Re}(C_n)\cos n\phi \\ &+ \sum_{n=0}^{\infty} \mathrm{Re}(D_n)\int_0^{2\pi} v_x(1,\phi')\cos n(\phi-\phi')d\phi' \\ &- \sum_{n=0}^{\infty} \mathrm{Im}(D_n)\int_0^{2\pi} w_x(1,\phi')\cos n(\phi-\phi')d\phi' \end{aligned} \tag{25}$$

and

$$\begin{aligned} \mathbf{n}\cdot\nabla^* w_x = &\sum_{n=0}^{\infty} \mathrm{Im}(C_n)\cos n\phi \\ &+ \sum_{n=0}^{\infty} \mathrm{Im}(D_n)\int_0^{2\pi} v_x(1,\phi')\cos n(\phi-\phi')d\phi' \\ &+ \sum_{n=0}^{\infty} \mathrm{Re}(D_n)\int_0^{2\pi} w_x(1,\phi')\cos n(\phi-\phi')d\phi' \end{aligned} \tag{26}$$

with the coefficients

$$C_n = \frac{\varepsilon_n i^n \omega R}{c}\left[J_n'\left(\frac{\omega R}{c}\right) - J_n\left(\frac{\omega R}{c}\right)\frac{H_n^{(1)'}\left(\frac{\omega R}{c}\right)}{H_n^{(1)}\left(\frac{\omega R}{c}\right)}\right] \tag{27}$$

and

$$D_n = \frac{\omega R\delta_n H_n^{(1)'}\left(\frac{\omega R}{c}\right)}{c\pi H_n^{(1)}\left(\frac{\omega R}{c}\right)} \tag{28}$$

Table 1. The Thermal and Dielectric Properties are Given for Oil and Water

Material Property	Oil	Water
Heat capacity, C_p [W s kg^{-1} °C^{-1}]	2000	4190
Thermal conductivity, k [W m^{-1} °C^{-1}]	0.168	0.609
Density, ρ [kg m^{-3}]	900	1000
Dielectric constant (2,450 MHz), κ'	2.80	78.10
Dielectric loss (2,450 MHz), κ''	0.15	10.44

and

$$\varepsilon_n = \begin{cases} 1, & n = 0; \\ 2, & \text{otherwise,} \end{cases} \text{ and } \delta_n = \begin{cases} 1/2, & n = 0; \\ 1, & \text{otherwise} \end{cases} \quad (29)$$

In Eqs. 27 and 28, J_n and $H_n^{(1)}$ are the Bessel and Hankel functions of the first kind, respectively, and prime indicates the first derivatives.

The electric field distributions within a sample in presence of reflective support need special mention. For 1-D slab, the reflective support is placed at the right end where $z' = 1$, hence the boundary conditions are $v_x = 0$ and $w_x = 0$. For a 2-D cylinder, the reflective support is the annular cylinder with radius R_a, such that at $R = R_a$, $v_x = 0$ and $w_x = 0$.

Dimensionless form of the energy balance equation in presence of microwave (Eq. 18), is

$$\overline{\rho C_p} \frac{\partial \theta}{\partial \tau} = \bar{k} \nabla^{*2} \theta + Q \quad (30)$$

where

$$\theta = \frac{T - T_\infty}{T_0}, \ \tau = \frac{\alpha_0 t}{D_s^2}, \ \overline{\rho C_p} = \frac{\rho C_p}{\rho_0 C_{p_0}}, \ \bar{k} = \frac{k}{k_0} \text{ and } Q = \frac{D_s^2 q}{k_0 T_0}$$

The initial condition for the entire sample (1-D slab or 2-D cylinder) is

$$\theta(\tau = 0) = 0 \quad (31)$$

In the analysis, an insulated boundary condition is used as

$$-\mathbf{n} \cdot \bar{k} \nabla^* \theta = 0 \quad (32)$$

where the insulated boundary condition is maintained at the faces for the 1-D slab, and at the outer surface for 2-D cylinders. The annular metallic cylinder as seen in Figure 1b is also maintained at the insulated condition. The insulated condition is imposed to analyze the heating effects due to heat generation only.

The coupled energy balance and the electric field equations with the appropriate boundary conditions are solved using Galerkin finite element method in the similar manner as discussed by Basak and Ayappa (1997, 2001).

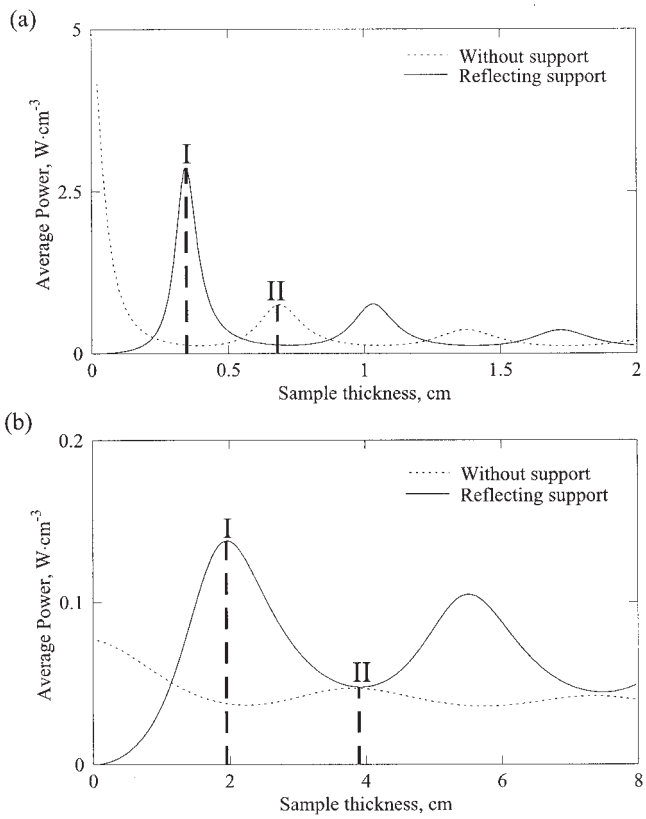

Figure 2. Average power (W · cm^{-3}) vs sample thickness for (a) water, and (b) oil samples. f = 2450 MHz, the incident MW intensity at left face, I_o = 1 W cm^{-2}.

The regime I corresponds to a maxima in average power for slabs with reflective support, and regime II refers to maxima for slabs without supports.

Results and Discussion

Microwave heating in 1-D slabs

A detailed analysis has been carried out to study the influence of reflective support on MW power distributions for oil and water samples. The simulation has been carried out mainly for oil and water samples as water is highly lossy substance while the oil has very small dielectric loss (see the properties in Table 1). In all cases the reflective support is placed at the unexposed face of 1-D slab where the slab is exposed to the MW radiation of intensity 1 W cm^{-2}.

A preliminary analysis on the role of reflective support is illustrated by average power distribution as a function of the sample thickness. The average power obtained from Eq. 14 is plotted as a function of sample thickness as seen in Figure 2. It is interesting to observe that the maxima in average power for slabs without support corresponds to the minima in average power for slabs with the support. As seen in Figure 2, the maxima in average power occurs at $2L = 0.5n\lambda_m$ where $n = 1, 2, \ldots$ for the slabs without support and the maxima corresponds to $2L = (0.5n - 0.25)\lambda_m$ for the slabs with support, where the wavelength of MWs within the samples, λ_m is defined in Eq. 16. Note that, the wavelength in the water sample is 1.38 cm, and that in oil is 7.3 cm. The occurrence of resonances of MW power is invariant with respect to dimen-

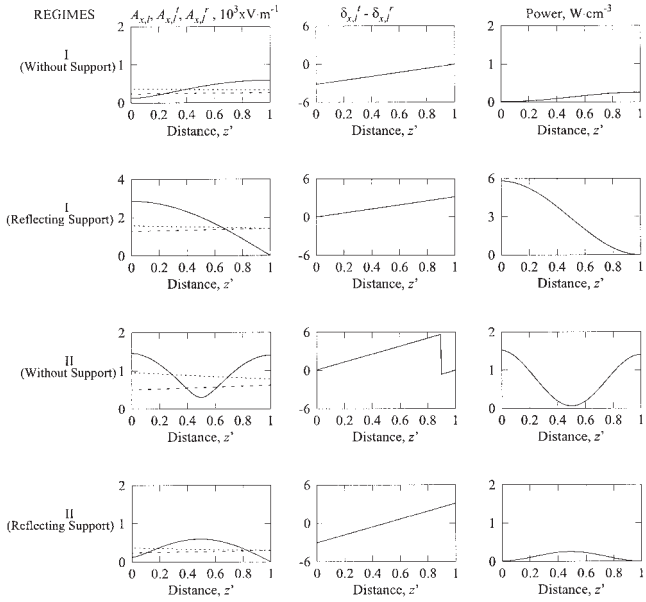

Figure 3. Amplitudes of electric field ($A_{x,l}$, $A_{x,l}^t$, $A_{x,l}^r$), phase difference ($\delta_{x,l}^t - \delta_{x,l}^r$) and power distributions for water slabs exposed to microwaves from the left face.

f = 2450 MHz, I_O = 1 W cm^{-2}. . . . , transmitted wave; – – –, reflected wave; —, stationary wave. For regime I, the maxima in power is observed at the unexposed face for slabs without support, and the maxima in power occurs at the exposed face for slabs with support. Greater spatial distributions in electric fields and power occur for slabs with support during regime I. For regime II, the maxima in power occur at both the faces for slabs without support and the only maxima in power occurs at the center for slabs with support. Greater spatial distributions in electric fields and power occur for slabs without support during regime II.

sionless length scales of materials as reported by Ayappa (1999).

We will consider two regimes (I and II) for both water and oil samples. The regime I corresponds to the maxima in average power in presence of support or the minima in absence of support while the regime II corresponds to the minima in presence of support or the maxima in absence of support. As seen in Figure 2a, the maxima in average power with support is considerably larger than the minima without support at regime I, while the difference in average power is smaller at regime II for water samples. In contrast, for oil samples, the average power at regime II is almost identical for the support and without support cases. In addition, the average power with support is greater than that without support for larger sample thicknesses of oil samples. These interesting features as seen in average power vs sample thicknesses for oil and water samples, thus, provide stimulus for determining the role of reflective supports on the efficient heating due to MWs. The detailed analysis on MW power characteristics and electric field distributions at various regimes would be useful to understand the interference of waves and the critical role of the reflective support.

Figure 3 illustrate the spatial distribution of electric fields and MW power absorption for regimes I and II in water samples. The MW power absorption of the stationary wave is analyzed, based on the influence of individual traveling waves due to transmission and reflection. We will carry out studies on the intensity of spatial resonance of absorbed power with spatial distributions of amplitudes ($A_{x,l}^t$; $A_{x,l}^r$; $A_{x,l}$), and the difference between phase angles ($\delta_{x,l}$) where amplitudes and difference between phase angles are obtained from Eqs. 8 and 9. As seen in Figure 2a, the processing length for regime I is 0.345 cm and that for regime II is 0.69 cm. For all the cases, it is observed that the amplitude of the transmitted wave, $A_{x,l}^t$ is greater than that of reflected wave, $A_{x,l}^r$. For regime I, the amplitude of the stationary electric field has a maxima at the unexposed face for the slabs without support, whereas the maxima occurs at the exposed face for the slabs with support. Note that, the phase difference between traveling waves being zero at the resonance corresponds to a maxima in amplitude of the stationary wave. The greater spatial distributions of stationary electric field and MW power are observed for the slabs with reflective support due to greater amplitudes of both the transmitted and reflected waves. For reflective supports, 80% of the sample absorbs greater power than that without support. It is interesting to note that, MW power varies between 0.01–0.25 W cm^{-3} for slabs without support whereas the power decreases monotonically from 5.8 W cm^{-3} for the slabs with support. In order to obtain a greater heating effect, a lossless ceramic (Al_2O_3) slab with 20% of the original slab thickness may be attached before the reflective support, and a detailed study may be a subject of future research.

Similar trend in distributions of transmitted and reflected electric fields is observed for regime II (see Figure 3). For regime II, the two maxima in stationary electric field occur at the faces of the slab without support, whereas a single maxima occurs at the center for the slab with support. The regime II corresponds a greater sample length which leads to greater MW power absorption for the slab without support. At the regime II, the smaller MW power deposition except at the center is observed for the slab with support. On the basis of regimes I and II, the efficient heating strategy would be guided by the role of the support for specific sample thickness for water samples.

Figure 4 illustrate the spatial electric fields and power distributions for oil samples. Similar to water samples, the maxima in MW power occurs at the unexposed face or the exposed face for regime I and for regime II the maxima occurs either at the faces or the center. Note that, the slab thickness for regime I is 1.9 cm, whereas the thickness for regime II is 3.8 cm. For oil samples, although the amplitudes of the transmitted and stationary electric fields are greater than that in water samples for all the regimes, the MW power absorption in the oil sample is smaller due to lower dielectric loss. For oil samples, the reflective support would always lead to a greater power absorption within the samples except at the unexposed face (for regime I), and at both the faces (for regime II). As oil absorbs less power than water samples, the greater thickness of oil can be processed and for all the cases reflective supports would be favored.

The thermal effect has been illustrated via temperature distribution as seen in Figure 5 for water samples. For all the cases, the sample is at 300 K prior to start the MW heating. Figures 5a and 5b represent the temperature distributions for regime I without support and with support respectively at various time intervals. We have shown temperature characteristics during 100 s, and it is found that the heating is extremely

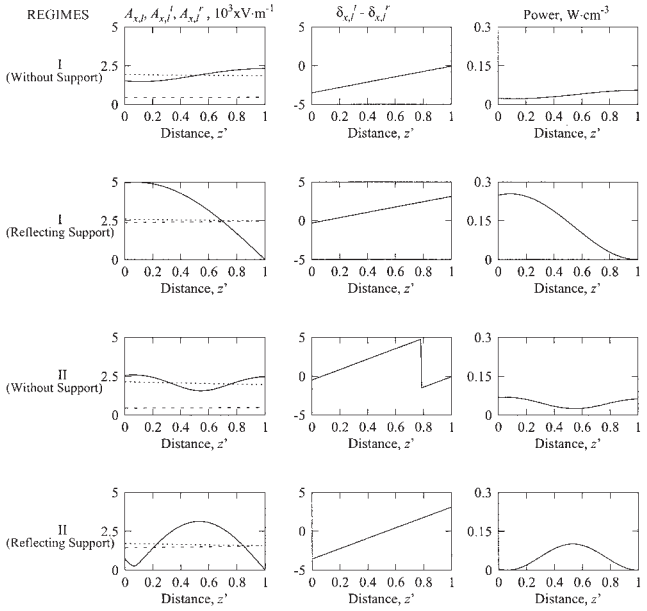

Figure 4. Amplitudes of electric field ($A_{x,l}$, $A_{x,l}^t$, $A_{x,l}^r$), phase difference ($\delta_{x,l}^t - \delta_{x,l}^r$) and power distributions for oil slabs exposed to microwaves from the left face.

f = 2450 MHz, I_O = 1 W cm^{-2}. . . . , transmitted wave; – – –, reflected wave; —, stationary wave. The qualitative behavior of spatial distribution fields and power is similar to that of water with identical situations. It is interesting to note that, for oil samples, the overall greater power absorption is observed for samples with supports during both regimes.

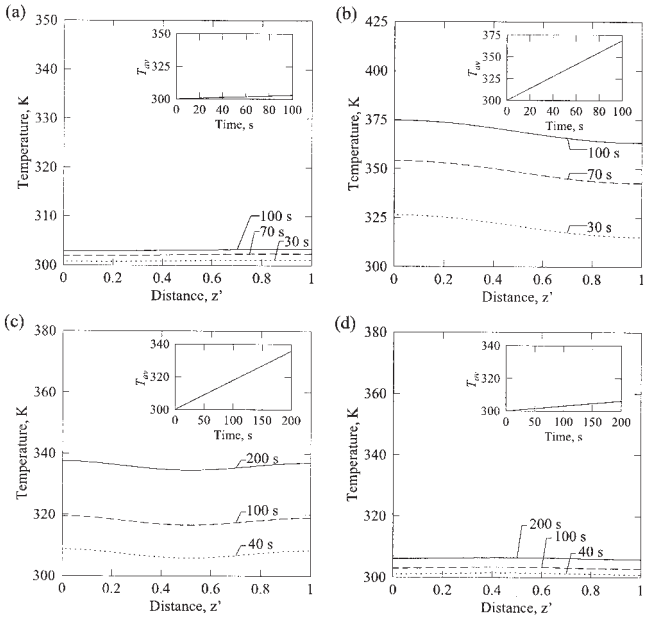

Figure 5. Temperature profiles in water slabs for (a) regime I, without support, (b) regime I, with support, (c) regime II, without support, and (d) regime II, with support.

The regime I (with support) and regime II (without support) correspond to greater spatial temperature distributions. The insets show the average temperature (T_{av}) vs time.

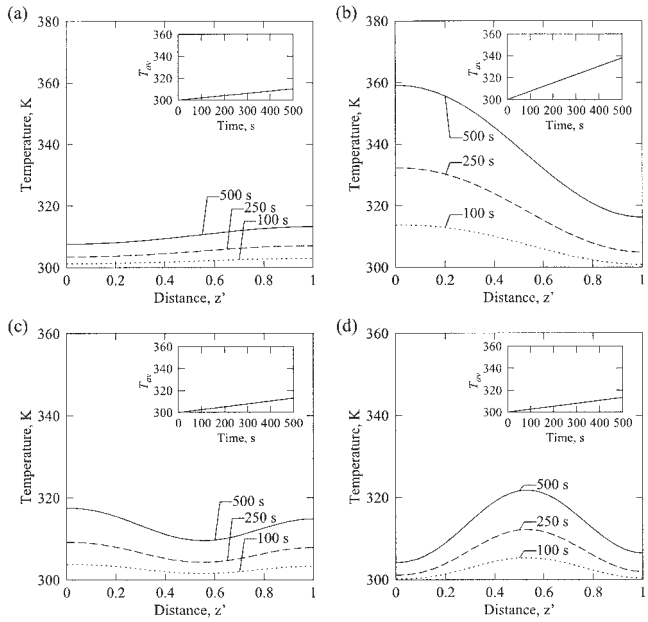

Figure 6. Temperature profiles in oil slabs for (a) regime I, without support, (b) regime I, with support, (c) regime II, without support, and (d) regime II, with support.

The temperature profiles are qualitatively similar to power profiles as seen in Figure 4. The maximum spatial temperature is achieved for samples with supports for both regimes I and II. The insets show the average temperature (T_{av}) vs time.

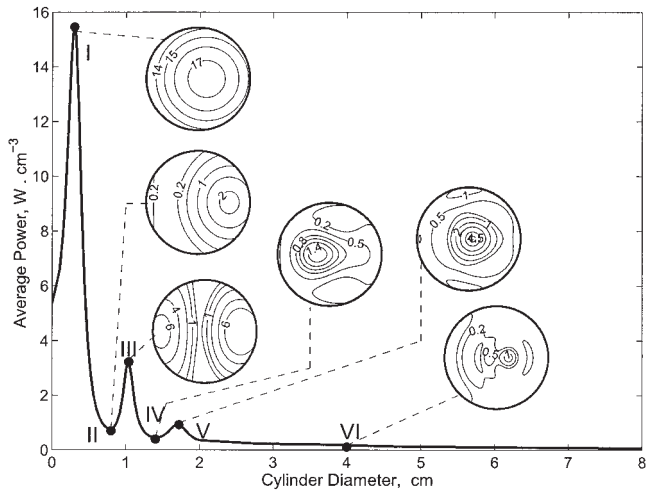

Figure 7. Average power (W · cm^{-3}) vs cylinder diameter for water samples without any support.

f = 2450 MHz, the incident MW intensity, I_O = 1 W cm^{-2}. The regimes I, III, V correspond to a maxima in average power and II, IV, VI denote the minima. The insets show the spatial variation in power for various regimes.

low for the slabs without support as maximum 3 K increase in temperature is found (Figure 5a). The spatial temperature distribution is almost uniform which signifies the low power depositions within the sample as seen in Figure 3. The scenario is completely different when the slab is heated with a support at the unexposed end. During 100 s, the highest temperature is

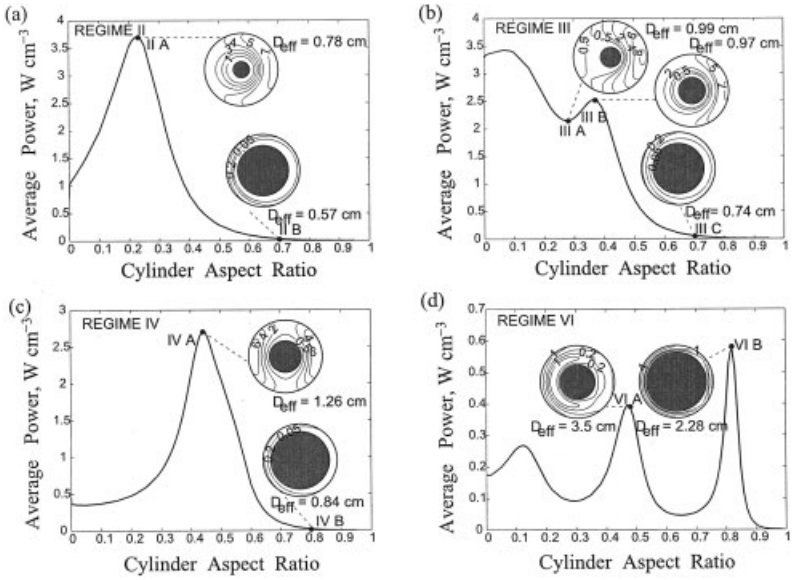

Figure 8. Average power (W · cm^{-3}) vs cylinder aspect ratio in water samples with supports for (a) regime II, (b) regime III, (c) regime IV, and (d) regime VI.

The maxima in average power is observed for intermediate aspect ratios. The insets show the spatial variation in power for various regimes and the shaded regimes in insets denote the annular metallic cylinder.

seen at the exposed end and the temperature varies within 363–375 K (Figure 5b). Although the unexposed end corresponds to zero MW power, the greater spatial power distribution at the rest of the samples contribute significantly for enhanced heating of the sample with the reflective support. At regime II, the slab without support exhibits greater heating effect than that with the reflective support (Figures 5c and 5d). During 200 s, the water sample without support heats up to 337 K whereas, the sample with support exhibits smaller heating effect with 5 K increase in temperature. The greater heating effect for regimes I and II are also pronounced via average temperature vs time plots (as seen in the insets) where the greater slopes are observed for slabs with support for regime I and without support for regime II.

Figure 6 illustrates the temperature distributions for oil samples. For all the regimes, the temperature distributions follow the trend similar to power distribution as seen in Figure 4. For regime I, heating rate is quite low as the temperature varies within 307–313 K during 500 s for the slab without support (Figure 6a). In contrast, during 500 s, the temperature could reach up to 360 K at the exposed end and a greater heating rate is observed up to 60% of the slab thickness with the reflecting support (Figure 6b). A greater heating rate leading to larger temperature distributions is also observed within the middle zone of the sample with support for regime II (Figures 6c and 6d). Overall, the enhanced heating in oil samples is due to the reflective support is observed. As seen in Figure 6d, based on the lower heating at the endpoints for regime II, the combined ceramic and reflective support could be a good choice in order to achieve a greater heating rate.

Microwave heating in 2-D cylinders

A detailed analysis on influence of reflective support has been investigated for 2-D cylinders where the reflective support is the annulus cylinder as shown in Figure 1b. The simulations are carried out to illustrate role of metallic support on enhanced heating strategies for both water and oil cylinders which are exposed to the MW radiation of intensity 1 W cm^{-2}.

A preliminary case study on microwave heating of water in the absence of support has been illustrated via average power vs cylinder diameter as shown in Figure 7. The average power for cylinders is obtained from the detailed solutions of electric field equations for cylinders as discussed in the Theory section. Here, the maxima and minima in average power are shown by regimes I to VI where regimes I, III, and V correspond to maxima, and II, IV, and VI correspond to minima. The spatial distributions of power at regime I show that entire sample absorbs considerably greater power for very small cylinders. At regime II, the minima in average power corresponds to a smaller deposition of power within the sample. The local maxima in power is observed near the unexposed face of the cylinder and a very low power absorption occurs at the exposed face. At regime III, the two maxima occurring at the exposed and unexposed faces cause a greater average power which contrast regime II. During regimes IV, V, and VI, the magnitudes of average power are smaller and the spatial distributions of power illustrate that only one maxima occurs at around the center of cylinder.

The overall power absorptions are considerably smaller at regimes II, IV, V, and VI as seen in Figure 7. Following our analysis on microwave heating of the 1-D slab with metallic support, the studies on heating of 2-D cylinders with metallic annulus would be important to investigate enhanced power absorption which are illustrated in Figure 8. Figure 8a illustrates the average power vs cylinder aspect ratio for regime II. The aspect ratio a, is defined as the ratio of radius of annulus (R_a) to radius of sample (R) and the effective diameter, D_{eff} of the sample with support is related with sample diameter $D = 2R$ as $D_{eff} = D\sqrt{(1 - a^2)}$. Note that, the samples without support corresponding to diameter D, and samples with sup-

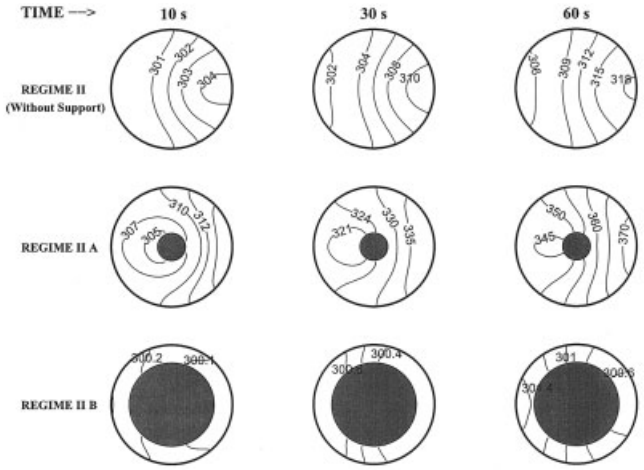

Figure 9. Temperature profiles in water samples for regime II (without support) and regimes II A and II B (with support).

Greater spatial temperature distributions are observed for regime II A.

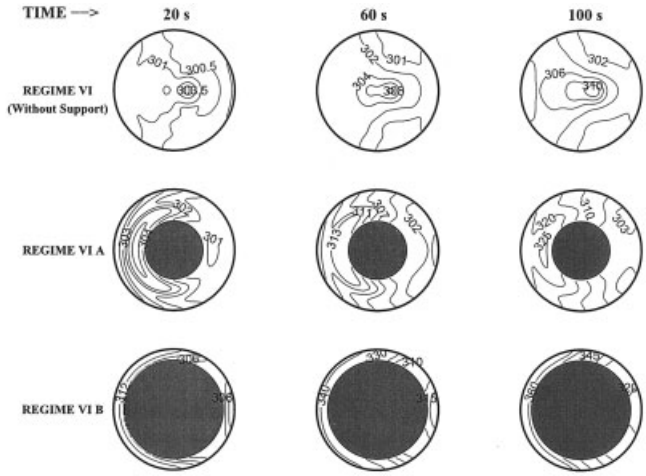

Figure 10. Temperature profiles in water samples for regime VI (without support) and regimes VI A and VI B (with support).

Greater spatial temperature distributions are observed for regimes VI A and VI B. Regime VI B corresponds to stratified and localized heating.

port corresponding to effective diameter D_{eff}, have the identical mass.

The average power has a maxima at $a = 0.23$ and the average power decreases with aspect ratio for $a > 0.23$, as seen in Figure 8a. It is interesting to note that, the average power for the sample is enhanced within a range of aspect ratio, 0–0.4. The minima in average power at regime II as seen in Figure 7 can be enhanced up to 3.7 W cm^{-3} corresponding to regime II A as seen in Figure 8a. In order to illustrate further the effect of metallic annulus, the spatial distributions of power are also shown at regime II A and II B. The spatial power distribution shows that a maxima 7 W cm^{-3} occurring at the unexposed face for the regime II A ($a = 0.23$, $D_{eff} = 0.78$ cm) which contrasts the maximum power 2 W cm^{-3} at regime II without any support with $D = 0.8$ cm as seen in Figure 7. The greater size of metallic cylinder may reduce the spatial power distribution as seen in the regime II B ($a = 0.70$, $D_{eff} = 0.57$ cm).

The influence of the metallic cylinder is also illustrated for other regimes. A number of local maxima is observed for cylinders at regime III where the primary maxima occurs at around $a = 0.1$, and a secondary maxima occurs at $a = 0.35$ (Figure 8b). To analyze the spatial power distributions, we identified three regimes as III A, III B, and III C. The spatial power distributions in regimes II A, III A, and III B are qualitatively similar and for all these cases a maxima in power occurs at the unexposed end. Regime III C corresponding to $a = 0.7$ leads to low spatial power deposition similar to II B. Note that, during regime III, except lower aspect ratio, the metallic support would lead to lower power absorption within sample. The average power absorption for samples without support in regimes IV and VI are lower as seen in Figure 8, and inclusion of metallic cylinder at the center increases the power by several times. As seen in Figure 8c, the average power and spatial power absorptions are greater at regime IV A ($a = 0.44$), and two maxima in spatial power are observed near both the exposed and unexposed faces. Two maxima in average power are also observed at regimes VI A and VI B as seen in Figure 8d. It is interesting to note that at greater aspect ratio ($a = 0.82$), the average power within the sample is greater than that without support and unlike other regimes II and III, the greater diameter of metallic annulus enhance the power deposition significantly for regimes VI A and VI B. This analysis also highlights that the MW processing of cylinders with larger size corresponding to regimes IV and VI can be enhanced significantly with annulus metallic cylinders of specific radii. The generalized analysis on enhanced microwave heating in Figure 8, thus provide a guideline on optimal use of metallic support for various regimes.

The enhanced heating effects due to the metallic support for water samples are illustrated in Figures 9 and 10. Note that, similar to 1-D samples, the heating studies are carried out with samples which are kept initially at 300 K. Figure 9 illustrates the temperature distributions for regime II (without support), and regimes II A and II B. As seen in Figure 7, a maximum in spatial power distributions occurs near at the unexposed face, and, consequently, the maximum temperature occurs near the unexposed surface and the temperature varies within 306–318 K during 60 s. In contrast, the metallic support corresponding to regime II A leads to a greater heating rate due to greater power absorption and during 60 s the enhanced heating rate would lead the temperature distributions within 345–370 K. The unexposed face reaches 370 K during 60 s, and this situation provides some interesting guideline to carry out localized heating of the sample with suitable metallic support. Note that, the negligible power absorption near to metallic wall does not influence significantly the temperature distributions, and due to conductive heat transport and the insulated boundary condition at the annulus, the temperature near the metallic wall increases up to 345 K. The lower power deposition during regime II B would heat within 300–301 K during 60 s.

Figures 10 illustrate the temperature distributions for regimes VI, VI A, and VI B. The maximum temperatures are

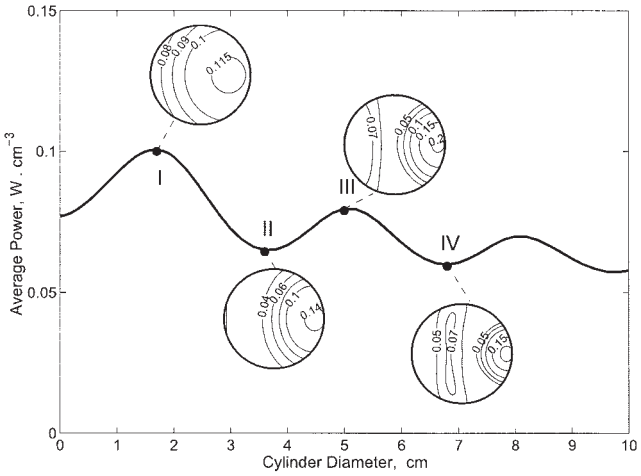

Figure 11. Average power (W · cm^{-3}) vs cylinder diameter for oil samples without any support. f = 2450 MHz, the incident MW intensity, I_O = 1 W cm^{-2}.

The regimes I and III correspond to maxima in average power, and II and IV denote the minima. The insets show the spatial variation in power for various regimes. An overall smaller power deposition for all the regimes is observed.

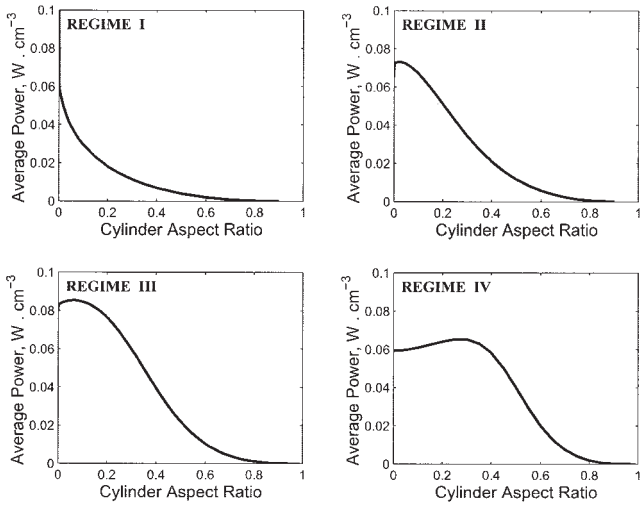

Figure 12. Average power (W · cm^{-3}) vs cylinder aspect ratio in oil samples with supports for regimes I, II, III, and IV.

The average power is seen to decrease with the aspect ratio except regime IV. The metallic annulus cylinder lowers the power absorption for oil samples in most of the cases.

observed at the center of the sample without support based on a greater power absorption as seen in Figure 7. During 100 s, it is observed that the highest temperature at the center is around 310 K when the sample is kept without any support. At regime VI A, a maxima in temperature is observed between the exposed face and the metallic wall and during 100 s, the sample reaches a local maxima of 325 K. During regime VI B (a = 0.82), the sample looks much thinner than the samples at regime VI A, and during 100 s, the stratification of temperatures is observed and the exposed face reaches around 360 K. For all the situations, the unexposed face always remains at a lower temperature than that at the exposed face which contrasts the situations at regimes II, II A, and II B. It is interesting to note that, the thicker metallic support enhances the heating rates for VI B contrasting the situation at regime II B, where the slowest heating rates are observed. For a faster thermal processing, the regime VI B may be a suitable choice whereas for a uniform heating, the samples corresponding to the regime II B may be preferred (Figures 9 and 10).

Figures 11 illustrate the average power vs cylinder diameter for oil samples. The maxima and minima in average power are shown by regimes I–IV where regimes I and III denote the maxima, and II and IV denote minima. The average power varies within 0.06–0.1 W cm^{-3} for all the regimes, and the spatial power absorptions for all regimes illustrate that the greater power deposition occurs at the unexposed face, and the spatial power distributions follow similar qualitative trend. The influence of metallic support has been examined for all the regimes as seen in Figure 12. For regimes I–III, it is observed that excepting the very low aspect ratios (for regimes II and III), the average power is a monotonically decaying function with the aspect ratio, and a slight increase in average power is observed at a = 0.4 for regime IV. Overall, it is interesting to note that, for oil samples, the inclusion of metallic support as an annulus cylinder would lead to lower heating effects which are in contrast with 1-D slabs. As oil reflects a significant amount of power and for 2-D geometries the enhancement of power due to metallic support may not be significant. The detailed analysis on enhanced heating due to a combined ceramic-metallic support would be a subject of future research.

Conclusion

We have carried out extensive studies to investigate the influence of reflective/metallic support on MW heating of 1-D and 2-D samples. The case studies were carried out for water, which has a greater dielectric loss and oil, which has low loss. A detailed mathematical analysis involving the roles of individual traveling waves, was carried out to illustrate the role of metallic support for 1-D slabs for both water and oil samples and rate of heating is obtained via solving energy balance equations. We have identified various regimes for optimal modes of operation with/without reflective supports, based on average power vs sample thickness diagram. The analysis has been extended for 2-D cylinders, where the support is placed as an annulus and the optimal microwave heating strategy depends on modes of operation, aspect ratio and sample diameter.

A preliminary analysis on the role of metallic support has been illustrated via average power vs sample thickness diagram for 1-D slab. We have identified two regimes I and II where regime I corresponds to a power maxima of the sample with support, and regime II corresponds to a maxima without support. For both these regimes and for both water and oil samples, it is observed that maxima in average power with/without support corresponds to minima in average power without/with support. It is interesting to note that for 1-D oil samples, except for lower sample thicknesses, the slab with metallic support exhibits greater average power. A detailed analysis on both the regimes for water and oil samples was carried out to illustrate the influence of metallic support via the role of individual

traveling waves. For regime I, it is observed that the amplitudes of transmitted and reflected electric fields are within the same order of magnitudes when the samples with the support are exposed to MWs. Note that, the spatial distributions of power show a maxima occurring at the unexposed face for samples without support and amplitudes of both transmitted and reflected fields are smaller throughout the samples for water and oil during regime I. In contrast, regime II illustrates that the samples without support has two maxima in spatial power as the amplitudes of both transmitted and reflected fields are greater, whereas the samples with support have one maxima in power at the center. The spatial distribution of MW power in oil is in general smaller and inclusion of metallic support seems to enhance the total electric field within oil samples for both regimes I and II.

The temperature distributions show that the enhanced heating rates for water samples with support for regime I where the temperature of the sample varies within 362–375 K during 100 s whereas for regime II, the temperature varies within 335–337 K during 200 s for samples without support. As the power absorption in a oil sample is smaller, during 500 s the oil samples heat up to 360 K for regime I and for regime II, the samples heat around 322 K. Note that, for oil samples, the maxima in spatial temperature with support is greater than that without support.

A preliminary analysis on MW power absorption for water samples in 2-D cylinder has been illustrated via average temperature via sample diameter diagram, where we have identified regimes I–VI where regimes I, III, and V denote the maxima and regimes II, IV, and VI denote the minima. The role of annulus metallic support has been illustrated for regimes II, III, IV, and VI. It is observed that for regime II, the average power is enhanced at $a = 0.23$, and for regime III, the average power is less with metallic support. As seen in Figure 7, the average power at regimes IV and VI is much smaller compared to that at regimes I–III. For both regimes IV and VI, the average power has been enhanced by few orders for intermediate aspect ratios. The heating rates are compared for samples with/without supports. The greater heating rates leading to greater temperature distributions within the sample corresponds to regime II A, and similarly, greater heating rates are observed for regimes VI A and VI B. In addition, a stratified and localized heating can be carried out using metallic annulus support as seen in regimes VI A and VI B. The average power distributions for an oil sample show very small power depositions for all regimes I–IV, and inclusion of metallic cylinder lowers the power deposition except the regime IV, where an intermediate aspect ratio corresponds to a small enhancement of power.

Literature Cited

Ayappa, K. G., H. T. Davis, G. Crapiste, E. A. Davis, and J. Gordon, "Microwave Heating: An Evaluation of Power Formulations," *Chem. Eng. Sci.,* **46**, 1005 (1991).

Ayappa, K. G., H. T. Davis, E. A. Davis, and J. Gordon, "Two-Dimensional Finite Element Analysis of Microwave Heating," *AIChE J.,* **38**, 1577 (1992).

Ayappa, K. G., "Resonant Microwave Power Absorption in Slabs," *J. Microwave Power and E. M. Energy,* **34**, 33 (1999).

Barringer, S. A., E. A. Davis, J. Gordon, K. G. Ayappa, and H. T. Davis, "Effect of Sample-Size on the Microwave-Heating Rate—Oil vs Water," *AIChE J.,* **40**, 1433 (1994).

Basak, T., and K. G. Ayappa, "Analysis of Microwave Thawing of Slabs With Effective Heat Capacity Method," *AIChE J.,* **43**, 1662, 7 (1997).

Basak, T., and K. G. Ayappa, "Influence of Internal Convection During Microwave Thawing of Cylinders," *AIChE J.,* **47**, 835 (2001).

Basak, T., and K. G. Ayappa, "Role of Length Scales on Microwave Thawing Dynamics in 2D Cylinders," *Int. J. Heat and Mass Transfer,* **45**, 4543 (2002).

Basak, T., "Analysis of Resonances During Microwave Thawing of Slabs," *Int. J. Heat and Mass Transfer,* **46**, 4279 (2003).

Basak, T., "Role of Resonances on Microwave Heating of Oil-Water Emulsions," *AIChE J.,* **50,** 2659 (2004).

Chamchong, M., and A. K. Datta, "Thawing of Foods in a Microwave Oven: I. Effect of Power Levels and Power Cycling," *J. Microwave Power and EM Energy,* **34**, 9 (1999).

Chatterjee, A., T. Basak, and K. G. Ayappa, "Analysis of Microwave Sintering of Ceramics," *AIChE J.,* **44**, 2302 (1998).

Jolly, P., and I. Turner, "Non-Linear Field Solutions of One Dimensional Microwave Heating," *J. Microwave Power and E. M. Energy,* **25**, 3 (1990).

Lee, M. Z. C., and T. R. Marchant, "Microwave Thawing of Cylinders," *Applied Math. Modelling,* **28**, 711 (2004).

Ohlsson, T., and P. O. Risman, "Temperature Distribution of Microwave Heating-Spheres and Cylinders," *J. Microwave Power,* **13**, 303 (1978).

Peschek, P., W. H. Atwell, M. Krawjecki, and G. Anderson, U. S. Patent No. 5140121 (1992).

Sivalingam, G., N. Agarwal, and G. Madras, "Kinetics of Microwave-Assisted Oxidative Degradation of Polystyrene in Solution," *AIChE J.,* **49**, 1821 (2003).

Weil, C. M., "Absorption Characteristics of Multilayered Sphere Models Exposed to UHF/Microwave Radiation," *IEEE Trans. Biomed. Eng.,* **BME-22**, 468 (1975).

Zhang, H., A. K. Datta, I. A. Taub, and C. Doona, "Electromagnetics, Heat Transfer, and Thermokinetics in Microwave Sterilization," *AIChE J.,* **47**, 1957 (2001).

Manuscript received Mar. 1, 2004, revision received Sept. 2, 2004, and final revision received Dec. 9, 2004.